Macromolecules

pubs.acs.org/Macromolecules Article

Mobility of Pressure-Densified and Pressure-Expanded Polystyrene Glasses: Dilatometry and a Test of KAHR Model

Xiao Zhao, Luigi Grassia, and Sindee L. Simon*

Cite This: *Macromolecules* 2021, 54, 8352–8364 Read Online

ACCESS | Metrics & More | Article Recommendations | Supporting Information

ABSTRACT: The structural recovery of pressure-densified (PDG) and, for the first time, pressure-expanded (PEG) glasses are experimentally investigated using pressurizable dilatometry. Both glasses show early devitrification on heating, indicating that these glasses have more mobility, compared to the conventional isobarically formed glass. The Kovacs–Aklonis–Hutchinson–Ramos (KAHR) model of structural recovery is able to reasonably predict the behavior of the pressure-expanded glass, but the KAHR model fails with the pressure-densified glass. The results suggest two limitations of the model: (i) the structural recovery is assumed to depend on the instantaneous liquid state and (ii) the same relaxation kinetics are assumed for the temperature and pressure perturbations. Modification of the KAHR model, allowing the departure from equilibrium, δ, to initially depend on the liquid state that the glass came from and to evolve toward the state that the glass is going to, improves the ability of the model to predict the early devitrification for the pressure-densified glass. Another modification of the KAHR model, allowing the temperature and pressure perturbations to relax independently of one another, results in effectively capturing the increased thermal expansion coefficient of glass lines during heating, as well as a "memory"-like aging behavior, for the pressure-densified glass.

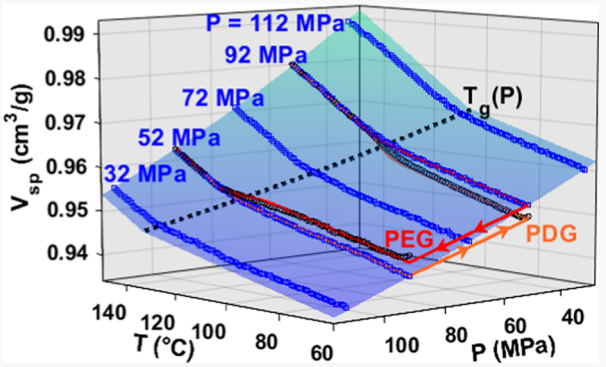

INTRODUCTION

A glass is formed by cooling a polymer or glass-forming liquid sufficiently fast and deep,[1−4] bypassing crystallization if it exists. The glassy state is a nonequilibrated state that spontaneously evolves toward the equilibrium or metastable equilibrium liquid state, with its density increasing[5,6] and with its fictive temperature,[7−10] T_f, decreasing, in a process that is known as structural relaxation.[11,12] Accompanying structural relaxation, the modulus and brittleness of glasses can increase significantly, leading to premature failure, even though the extent of densification is generally less than 1%.[1,12−17] Consequently, understanding the nonequilibrium segmental or molecular mobility that determines structural relaxation of glassy materials is important to facilitate modeling and ultimately the design of glasses with better properties and increased reliability.

The kinetics of structural recovery are widely described by the phenomenological Kovacs–Aklonis–Hutchinson–Ramos (KAHR)[18] model or the equivalent Tool–Narayanaswamy–Moynihan (TNM)[7,8,19] model, where the mobility is characterized by the magnitude and distribution of the relaxation time, τ. The KAHR and TNM models are able to describe the representative "Kovacs Signatures" aging experiments,[5,6,20] enthalpy overshoot,[10,21] pressure-dependent structural relaxation,[22−24] and pressure-jump-induced volumetric recoveries.[25]

However, the KAHR/TNM structural recovery model predictions for a combination of temperature and pressure cycles are still challenging, including for the pressure-densified glass (PDG), which is formed by first vitrifying a liquid at a high pressure, P_1, followed by depressurizing the high-pressure glass to a low pressure, P_2, with the resulting glass having a higher density in comparison to the corresponding conventional glass (CG) that is isobarically formed at P_2. PDG is common in injection molding[26] and has been studied for various glass-forming materials, including but not limited to water,[27] phenolphthalein,[28] glycerol,[29] polystyrene,[30−33] poly(methyl methacrylate),[30,34−36] poly(vinyl chloride),[33,37] and polycarbonate.[37,38] In spite of its high density, PDG shows weakened yield stress,[39] manifests a loss of latent heat during heating,[40] and becomes more ductile during aging.[41] Importantly, structural recovery at temperatures even 50 °C below the glass-transition temperature, T_g, is observable for PDG, both macroscopically[30] and microscopically,[42] indicating

Received: May 4, 2021
Revised: July 31, 2021
Published: September 10, 2021

https://doi.org/10.1021/acs.macromol.1c00983
Macromolecules 2021, 54, 8352–8364

that PDG is an 'unstable' densified material, having anomalously high segmental or molecular mobility in spite of its higher density.

The increased mobility for PDG has been demonstrated in various experimental studies, including but not limited to scattering characterization,[38,42−46] mechanical testing,[39,41,47,48] dielectric spectroscopy,[36,49−51] thermal conductivity,[29,52] calorimetry,[30,39−41,46,53] and dilatometry,[30,32,34,35,38,39,41,54] of which the last one, the dilatometric method, allows one to perform *in situ* pressure jumps and thermal cycles and to measure the anomalous pressure−volume−temperature (PVT) behavior of the PDG in comparison to the corresponding CG. When heating a PDG from the glassy to the liquid state, dilatometric studies show devitrification prior to T_g accompanied by little or no overshoot of the extrapolated liquid line,[39,55] whereas an aged (or densified) CG overshoots the extrapolated liquid line at T_f and devitrifies at temperatures above the nominal T_g. Moreover, during heating, the apparent thermal expansion coefficient for PDG is higher than that for CG in the glassy region.[39,41] Recently, Holt et al. have shown similar observations from dilatometric studies on polycarbonate[38] and 1,3,5-tri(1-naphthyl)benzene,[54] and for the latter molecular glass, they also demonstrated "memory"-like aging behavior of the PDG, where the volume first expands to the level of the relaxation of CG followed by a conventional contraction analogous to the isobaric temperature jump-indued memory effect;[10,56,57] a similar "memory effect" was also observed by Pae and Vijayan[48] in terms of the evolution of Young's modulus for PDG.

The ability to model the behavior of PDG is important not only for fundamental understanding but also for describing materials made through the injection molding process. Weitz and Wunderlich[30] combined the simple hole theory of Hirai and Eyring,[58] which correlates the reduction of enthalpy accompanied by the compressed volume, with a two-state energy model, which assumed that the PDG inherited the higher energy configuration of the liquid state where the glass was vitrified; the model qualitatively predicted the enthalpy elevation of the PDG, but the prediction leveled off as pressure increased and the method overestimated the extent of densification by roughly 3-fold. The relaxation dynamics of the PDG, however, were not modeled by Weitz and Wunderlich.[30] Holt et al.[54] were able to qualitatively capture the signature of "memory"-like behavior for the PDG by modifying the KAHR model with τ described by thermodynamic scaling,[59] *i.e.*, $\tau \propto TV^{\gamma}$, but the magnitude of the initial expansion was not captured, with a discrepancy between the prediction and data presumably related to the assumption of the same relaxation kinetics for temperature and pressure perturbations (as will become obvious later). They also were unable to capture the early devitrification. In the present study, we further examine the limitations of the classic KAHR structural recovery model to predict the PVT behavior for the PDG. Two modifications, in particular, are investigated: (i) we allow the relaxation time to depend on the departure from a phantom equilibrium state that evolves with time from the liquid line where the glass was vitrified toward the liquid line where the glass is devitrified, and (ii) we allow the relaxation kinetics associated with temperature and pressure perturbations to relax independently.

In addition to the experiments and modeling of the PDG, we also investigate a pressure-expanded glass (PEG) that is formed by first vitrifying a liquid at a low pressure, P_1, followed by pressurizing the low-pressure glass to a high pressure, P_2, with the resulting glass having a lower density[60] in comparison to the corresponding CG that is isobarically formed at P_2. Pressurizing a low-pressure glass is one of the three approaches to obtain different glasses as was investigated and summarized by McKinney and Goldstein,[61] of which the other two ways are depressurization of a high-pressure glass to form PDG and isobaric vitrification to form CG. Moreover, the compression of isobarically formed glass is often performed in order to obtain the bulk modulus of a polymer glass.[62−66] However, studies of the volumetric recovery of the PEG have not been conducted to the best of our knowledge, nor has this behavior been predicted by the KAHR or TNM models of structural recovery. Here, the nonequilibrium dynamics of the PEG during heating are investigated and compared to that for the PDG, in order to reveal the nature of the hydrostatic influence on the segmental or molecular mobility of glass-forming materials. We note that Andersson and Johari[29,52] recently proposed and investigated the evolution of thermal conductivity during heating of a pressurized ambient glass, equivalent to the pressure-expanded glass defined in the current study. They observed that the thermal conductivity of the PEG was lower than that of the corresponding CG.

In the present study, the segmental mobility of polystyrene PDG and, for the first time, PEG is experimentally investigated during heating and isothermal aging. The pressure and thermal cycles and volumetric measurements are conducted *in situ* using a custom-built pressurizable dilatometer in our laboratory, which applies pressure to the sample using a confining fluid resulting in a uniform hydrostatic pressure in the sample, regardless of its state (*i.e.*, liquid or glass);[67] the instrument has been successfully applied to measure the PVT behavior and pressure relaxation for linear[68,69] and star[70] polystyrene, cyanurate networks,[71,72] and a polystyrene nanocomposite.[73,74] The structural relaxation for the isobaric and nonisobaric thermal histories are described using the KAHR structural recovery model in order to demonstrate its limitations, and two novel modifications of the KAHR model are made that allow quantitative description of experimental observations.

METHODOLOGY

Material. A narrow-distribution high-molecular-weight atactic polystyrene (PS) powder (Scientific Polymer Products, Inc.) is used for the studies with a weight-average molecular weight of 2 257 000 g/mol and a number-average molecular weight of 1 928 000 g/mol. The polystyrene powder is degassed in a vacuum oven for 3 days followed by loading into a cylindrical mold with a diameter of 4.02 mm under N_2 atmosphere. The sample is molded at 200 °C under vacuum, followed by cooling at 0.10 K/min to room temperature. T_g of the raw polystyrene powder and the molded rod are 101.1 ± 0.1 and 100.8 ± 0.4 °C, respectively, based on differential scanning calorimetry measurements made on heating after cooling at 10 K/min, indicating no significant degradation. The sample rod is machined to reduce its diameter to 3.90 mm and then is annealed in the mold at 120 °C for 2 h under vacuum. Eight sample rods with an atmospheric density of 1.0410 ± 0.0019 g/cm^3 and a total mass of 1.0449 ± 0.0001 g are loaded into the sample cell of our custom-built pressurizable dilatometer for the pressure−volume−temperature (PVT) measurements. Before and after the measurements, no bubbles or defects were observed in the sample.

https://doi.org/10.1021/acs.macromol.1c00983
Macromolecules 2021, 54, 8352−8364

Dilatometry. The setup and performance of the custom-built pressurizable dilatometer have been described elsewhere,[69] but for the sake of completeness, we briefly describe the instrument here. The sample cell has a cylindrical interior space of 100 mm × ø4.8 mm, giving a volume of approximately 2.0 cm^3, and is filled with Krytox GPL107 fluorinated synthetic oil, which is the sample-confining and pressure transmitting fluid. The sample cell is completely immersed in a Hart Scientific 6024 oil bath, which uses Dow Corning 200 Fluid 100 CST silicone oil and maintains a temperature stability better than 0.01 °C. The pressure is controlled through a high-pressure piston connected to a stepper motor, with the displacement of the piston shaft measured using an Omega Engineering linear variable differential transducer (LVDT). We note that the LVDT data is used only from −4 to 7 V, with data from −7 to −4 V omitted due to an unknown instrument issue. The temperature of the sample is measured using a thermocouple attached to the sample cell. The pressure of the entire system is measured by a Honeywell TJE 60000 PSI pressure transducer. Data acquisition and automation control are implemented using a LabVIEW program.

The PVT behavior of our PS sample is measured for the following pressure and thermal histories:

- Isobaric cooling and heating scans are performed at 0.10 K/min from 170 toward 40 °C and then back to 170 °C for pressures of 32, 52, 72, 92, and 112 MPa, with a hold of 60 min at the lower temperature in order to ensure that the temperature is well controlled prior to heating, since the cooling rate of 0.10 K/min cannot be maintained below 60 °C. A representative temperature vs time history is shown in the Supporting Information.
- Isothermal pressure scans are performed to obtain the bulk modulus in the liquid and glassy state, at 160 and 60 °C, respectively. For the liquid state, the system is held at the constant temperature of 160 °C, and the specific volume is measured for pressures from 15 to 138 MPa, using a pressurization rate of 0.40 MPa/min. For the glassy state, Struik's protocol[75] is followed in order to ensure that structural relaxation does not influence the data. Hence, the experiment is composed of three steps: (i) isobaric cooling at 0.10 K/min from 170 to 60 °C at P_1 = 52 or 92 MPa, (ii) a hold of 1000 min at 60 °C, and (iii) a pressure scan at 0.40 MPa/min toward P_2 = 92 MPa for P_1 = 52 MPa and a scan toward P_2 = 52 MPa for P_1 = 92 MPa.
- Nonisobaric thermal histories are performed to prepare and characterize the pressure-densified and pressure-expanded glasses. These histories are composed of three steps: (i) cooling at 0.10 K/min from 170 to 60 °C at P_1, (ii) application of a pressure jump from P_1 to P_2 at 60 °C, with pressurization or depressurization applied over 10 min in an evenly stepwise manner (using 5 steps), and (iii) heating at 0.10 K/min from 60 to 170 °C at P_2. Pressure down-jump experiments were made for P_1 = 92 MPa to P_2 = 52 and 72 MPa at 60 °C, forming pressure-densified glasses, PDG-52 and PDG-72; and pressure up-jump experiments were made from P_1 = 52 MPa to P_2 = 72 and 92 MPa at 60 °C, forming pressure-expanded glasses, PEG-72 and PEG-92. An average rate of pressure change is anticipated to represent the actual pressurization or depressurization rate because of the relatively short time coupled with the sample being deep in the glassy state.
- Two aging experiments at 112 °C and 52 MPa are performed for 6 days (5.36×10^5 s), one for CG after a temperature down-jump and one for a PDG after a more complicated thermal history. For the CG, the sample is cooled at 0.10 K/min from 170 to 112 °C at 52 MPa, followed by isothermal, isobaric aging. For the PDG, the history includes (i) cooling to deep in the glassy state at 0.10 K/min from 170 to 60 °C at P_1 = 92 °C, (ii) performing a pressure jump to form the PDG at on average 4 MPa/min from P_1 = 92 °C to P_2 = 52 MPa, (iii) heating to the aging temperature at 0.10 K/min from 60 to 112 °C at P_2 = 52 MPa, and then (iv) isothermal, isobaric aging at 112 °C and 52 MPa.

Equation of State. The PVT data in the liquid state and the data of isobaric temperature scans in the glassy states are separately described by the Tait equation of state[76,77]

$$V(P, T) = V(P_a, T)\left\{1 - C_0 \ln\left[1 + \frac{P}{C_1 \exp(-C_2 T)}\right]\right\} \quad (1)$$

where C_0, C_1, and C_2 are material-dependent parameters, and C_0 is taken to be 0.0894,[78] as is often the case for polymers. Here, the pressure and temperature are in the units of MPa and °C, respectively. For the liquid state, the atmospheric specific volume is expressed as the reciprocal of a polynomial function of temperature, consistent with previous work[69,70,72,74]

$$V(P_a, T) = \frac{1}{a_0 + a_1 T + a_2 T^2} \quad (2)$$

where a_0 is the reference density at 0 °C, and a_1 and a_2 are material-dependent constants. For the glassy state, the atmospheric specific volume is expressed as a reciprocal of an exponential function of temperature

$$V(P_a, T) = \frac{1}{a_0 \exp(a_1 T)} \quad (3)$$

where a_0 is the reference density at 0 °C and a_1 is equivalent to the coefficient of thermal expansion. Although eq 3 is often used to describe the atmospheric liquid volume as well, we have found that the difference between eqs 2 and 3 for PS is negligible for the temperature range of interest.[79]

KAHR Model. The KAHR[18,24] structural recovery model is used to describe the isobaric cooling and heating scans together including the liquid, glass transition, and glassy regions. The model assumes additivity of the contributions of temperature and pressure perturbations to the total volume, $V(t)$

$$V(t) = V_0 + \int V(t)\{\alpha_{glass} + \Delta\alpha[1 - M(t, t')]\}dT + \int V(t)\{\beta_{glass} + \Delta\beta[1 - M(t, t')]\}dP \quad (4)$$

Here, V_0 is the initial volume in the equilibrium liquid state, and $\Delta\alpha$ and $\Delta\beta$ are the change in the thermal expansion coefficient and isothermal compressibility between the liquid and glassy states, *i.e.*, $\Delta\alpha = \alpha_{liquid} - \alpha_{glass}$ and $\Delta\beta = \beta_{liquid} - \beta_{glass}$, respectively, and are determined from the Tait equation with the exception of β_{glass}, which is determined from the

https://doi.org/10.1021/acs.macromol.1c00983
Macromolecules 2021, 54, 8352−8364

isothermal pressure scans in the glassy state at 60 °C since that is the temperature at which pressure jumps are made and since the Tait equation for the glass cannot provide that value. We note that in previous work on another polystyrene using capillary dilatometry,[9] $\Delta\alpha$ was independent of cooling rate over a range of cooling rates from 0.003 to 0.1 K/min; in that work, however, we did observe a slightly lower value of α_{glass} on heating compared to cooling, but that difference is not observed here because the pressurizable dilatometer used in this work covers a broader range of volumes and hence is less sensitive than the capillary dilatometer. $M(t, t')$ is the response function for the perturbations with respect to the reduced time from t' to t, accounting for the time-dependent relaxation from the instantaneous glassy response to the long-term liquid response. Notably, the same relaxation kinetics are conventionally assumed for both temperature and pressure perturbations (although this requirement is relaxed later) with $M(t, t')$ expressed by the stretched exponential Kohlrausch–Williams–Watts function[80,81]

$$M(t, t') = \exp^{-\left(\int_{t'}^{t} d\xi/\tau\right)^{B}} \quad (5)$$

where τ is the relaxation time and B is the stretched exponent that determines the distribution of τ, which is considered to be equivalent to a summation of the weighted exponential response functions each with a unique τ, as shown by Kovacs et al.[18]

The magnitude of τ depends on T, P, and δ, the departure from the equilibrium

$$\ln \tau = \ln \tau_{ref} + \theta_T(T - T_{ref}) + \theta_P(P - P_{ref}) + \theta_\delta\delta \quad (6)$$

$$\theta_\delta = (1 - x)\theta_T/\Delta\alpha \quad (7)$$

and

$$\delta = (V - V_e)/V_e \quad (8)$$

Here, τ_{ref}, θ_T, θ_P, and x are material-dependent adjustable parameters; V_e is the corresponding equilibrium state at the instantaneous T and P, and is extrapolated from the liquid Tait equation; and the reference state is chosen as T_{ref} = 118 °C and P_{ref} = 72 MPa. Values of the τ_{ref}, θ_T, θ_P, x, and B parameters can be obtained experimentally or by fitting,[82] and in the present study, we fit to the PVT data and make comparisons to the literature. The KAHR model eqs 4 and 5 are solved numerically, with the step size equal to 6 *sec* such that the corresponding volumetric step changes are less than 5×10^{-6} and 8×10^{-5} cm^3/g for temperature and pressure perturbations, respectively.

RESULTS

Isobaric cooling and heating scans at 0.10 K/min are performed at 32, 52, 72, 92, and 112 MPa. The average of four scans at each pressure (except for the scans at 112 MPa that are conducted twice) is plotted in Figure 1, and the standard deviation of each dataset is provided in Table 1. The standard deviation results of the isobaric scans in the present study are the same order of magnitude ($\sim 10^{-4}$ cm^3/g) as those for the previous dilatometric isobaric scans for other polymeric materials measured in our laboratory.[69,72,74] In Figure 1, both the cooling and heating scans show a linear dependence on temperature in both liquid and glassy regions, and a linear extrapolation is used to determinate the experimental T_g as the point of intersection. The experimental T_g values are plotted as

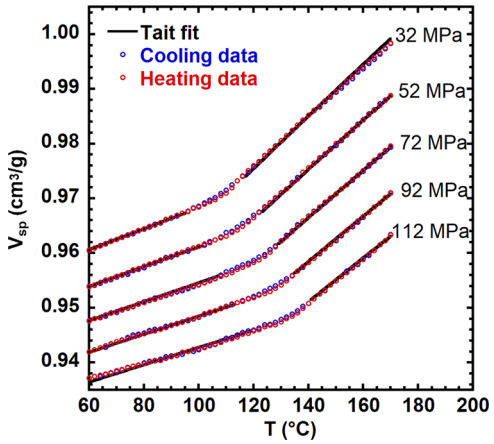

Figure 1. PVT data for the isobaric cooling and heating scans at 0.1 K/min at 32, 52, 72, 92, and 112 MPa. For each pressure, the data are the average of four separate runs, except for the data at 112 MPa which are two. Also shown are the predictions of the Tait equation, fit separately in the liquid and glassy regimes.

a function of pressure in Figure 2. The pressure dependence of T_g is found to be 0.30 °C/MPa in Figure 2 and agrees well with the literature,[32,68,83−85] where values range from 0.25 to 0.36 °C/MPa for polystyrene.

The volumetric results for the isothermal pressure scans at 160 °C are plotted in Figure 3 against pressure, using several different masses of hydraulic fluid in order to cover a broad pressure range from 15 to 138 MPa. Also shown in Figure 3 is the volume at 160 °C and P = 32, 52, 72, 92, and 112 MPa from the isobaric scans, which agrees well with the isothermal pressure scan data. For each mass of hydraulic fluid loading, a few data points at the lower-pressure end of each measurement deviate from the overall dependence due to the LVDT issue mentioned in the Methodology.

The isobaric cooling and heating scans and the isothermal pressure scans in the liquid state are simultaneously fitted by the Tait equation, and the results are shown as solid lines in Figures 1 and 3. The Tait equation is also fit to the glassy isobaric data, as shown in Figure 1. For both liquid and glassy states, the Tait equation well describes the experimental results with a fitting error of ±0.00023 cm^3/g. The Tait equations can also describe the pressure-dependent T_g, determined as the intersection of the liquid and glass lines, as shown by the dashed line in Figure 2. Values of the Tait parameters, along with sample molecular weight and T_g, are compared to the literature in Table 2. For the liquid state, the reference density at 0 °C, a_0, is within 1% of the literature values.[62,69,86] In addition, the liquid thermal expansion coefficient, $\alpha = (\partial \ln V/\partial T)_P$, determined using the isobaric data 10 to 40 °C above T_g, is compared to data in the literature in the Supporting Information (Figure S2) with values being the same within the error of the measurements as those reported by Meng et al.,[69] Quach and Simha,[62] and Zoller and Hoehn[86] at pressures below 60 MPa. Our observed pressure dependence of the liquid thermal expansion coefficient is weaker than in those works, resulting in a higher liquid thermal expansion coefficient at 112 MPa, but our value is still within the range of data reported by Oels and Rehage.[32] The liquid bulk modulus, $K = -(\partial P/\partial \ln V)_T$, is determined using the pressure scan data at 160 °C; our values are within 10% of those reported by Meng et al.,[69] Quach and Simha,[62] and Zoller and Hoehn,[86] as shown in Supporting Information Figure S3, with our pressure

https://doi.org/10.1021/acs.macromol.1c00983
Macromolecules 2021, 54, 8352−8364

Table 1. Standard Deviation among Multiple Runs for Isobaric Cooling or Heating Scans and the Representative Nonisobaric Thermal Histories [cm^3/g]

	isobaric cooling scans and heating scans for indicated pressures [MPa]					nonisobaric thermal histories	
	32	52	72	92	112	PDG-72	PEG-72
cooling	0.00036	0.00043	0.00030	0.00065	0.00032	N/A[a]	N/A[a]
heating	0.00020	0.00034	0.00019	0.00043	0.00034	0.00017	0.00045

[a]Results for the cooling are equivalent to those for the isobaric cooling scans at 72 MPa.

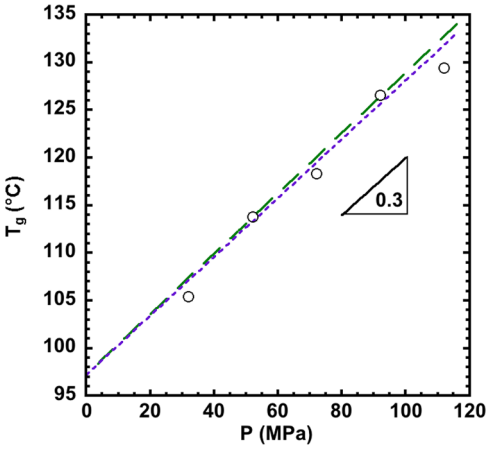

Figure 2. T_g as a function of pressure for the isobaric temperature scans: data (circles) and predictions of the Tait equation extrapolation (green dashed lined) and the KAHR model (purple dashed line).

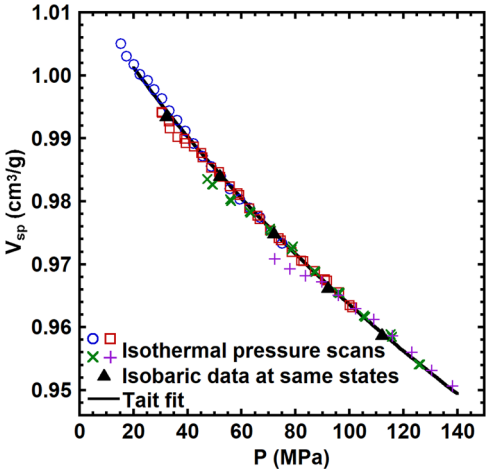

Figure 3. PVT data for isothermal pressure scans at 160 °C with various loads of the hydraulic oil: 5.40 g (blue circles), 5.56 g (red squares), 5.69 g (green axes), and 5.87 g (purple pluses). Also shown are the PVT data for isobaric temperature scans at 160 °C (triangles), as well as the prediction of the Tait equation (line).

dependence being approximately 15% higher. For the glassy state, a_0 is between 0.6 and 1% lower than the others,[62,69,86] indicating a higher glassy volume, which is presumably due to the higher T_g resulting from the higher molecular weight of our sample studied here. The glassy α in our work is determined using the isobaric data 15 to 45 °C below T_g, and the result, from 32 to 112 MPa, is slightly lower but within 10% of the literature values,[32,62,69,86] as shown in Figure S2. Our glass bulk modulus, shown in Figure S3 as a function of pressure, is determined using the pressure scan data at 60 °C, and is between Meng et al.'s results at 35 and 60 °C, with an extrapolation to atmospheric pressure of 2.7 GPa that is same as that extrapolated by Meng et al.[69] Notably, parameter C_1 in Tait equation is equivalent to the effective bulk modulus for the set of isothermal data, and our glassy value in Table 2 is consistent with Meng et al.[69] and is lower than the others because both Quach and Simha[62] and Zoller and Hoehn[86] obtained the set of isothermal data using pressure jumps from a low-pressure glass, whereas ours are from isobaric scans at the same temperature.

On the other hand, the Tait equation can only describe the PVT data in liquid and glassy states and cannot capture the kinetics associated with the glass transition, including changes in the level of glass lines for different cooling rates, as well as undershoots and overshoots at T_g on heating. In order to capture such kinetics associated with vitrification and devitrification phenomena, the isobaric cooling and heating scans are further described from the liquid to the glassy states by the KAHR model, with the pressure-dependent $\Delta\alpha$ determined using the Tait equation. Predictions of the KAHR model are shown as solid lines in Figure 4, along with the isobaric cooling and heating scan data. The KAHR model quantitatively describes the pressure-dependent glass transition and the level of glass lines, giving a fitting error of ±0.00070 cm^3/g. Values of the KAHR model fitting parameters are reported in Table 3, with the values of θ_T, x, and B in good agreement with the literature values;[5,57,87,88] θ_T can also be approximated by $\Delta H/RT_g^2$, where the parameter ΔH is used in the equivalent TNM model. Although the reported values for θ_P are rarely founded in the literature, our result is the same order of magnitude as that reported by Tribone et al.[25] (≈0.1 MPa^{-1}) for polystyrene, and is similar to the value reported by Simon et al.[22] (=0.2 MPa^{-1}) for ortho-terphenyl. The KAHR model predicts the pressure-dependent T_g, also determined as the intersection of the liquid and glass lines, as shown by the dotted line in Figure 2, consistent with the experimental results and the Tait predictions.

The PVT behavior of the pressure-densified and pressure-expanded glasses on heating are plotted against temperature in Figures 5 and 6, respectively, along with the corresponding isobaric cooling and heating scan data for the conventional glass. As expected, the densities of the PDG in the glassy state are higher than those of the corresponding CG, whereas the densities of the PEG are lower. The extent of densification (or expansion) is given by the densification compressibility, as introduced by McKinney and Simha[83]

$$\text{densification compressibility} = \frac{V_{CG} - V_i}{V_{CG}\Delta P} \tag{9}$$

where V_{CG} is the volume of the corresponding CG, V_i is the volume of the PDG or PEG right after the pressure jump, and ΔP is the size of the pressure jump. The densification compressibility for the two PDGs and the two PEGs are plotted against ΔP, in Figure 7, along with results from the literature for polystyrene (PS)[30,43] and poly(vinyl acetate)

https://doi.org/10.1021/acs.macromol.1c00983
Macromolecules 2021, 54, 8352−8364

Table 2. Parameters of the Tait Equation for Polystyrene, along with Sample Molecular Weight and T_g, Compared to Values Reported in the Literature

	this study	Meng et al.[69]	Quach and Simha[62]	Zoller and Hoehn[86]
M_n (kg/mol)	1,928	92.8	90.7	30
atmospheric T_g (°C)	97[a]	93.8	92	79.3
rate to obtain T_g (°C/min)	0.1	0.1	0.17	0.5
		Liquid State		
a_0 (g/cm^3)	1.0773	1.077	1.077	1.067
$a_1 \times 10^4$ (g/(cm^3 °C))	−6.3085	−4.99	−5.49	−5.02
$a_2 \times 10^7$ (g/(cm^3 °C^2))	3.9456	−2.08	1.24	−1.35
C_1 (MPa)	195.23	216.9	216.9	257.1
$C_2 \times 10^3$ (°C^{-1})	2.2801	3.5	3.32	4.08
		Glassy State		
a_0 (g/cm^3)	1.0414	1.052	1.048	1.052
$a_1 \times 10^4$ (°C^{-1})	−2.1341	−2.37	−2.68	−2.86
C_1 (MPa)	235.46	208.5	344.9	399.4
$C_2 \times 10^3$ (°C^{-1})	1.3695	1	2.71	4.31

[a]Extrapolated from T_g vs P data.

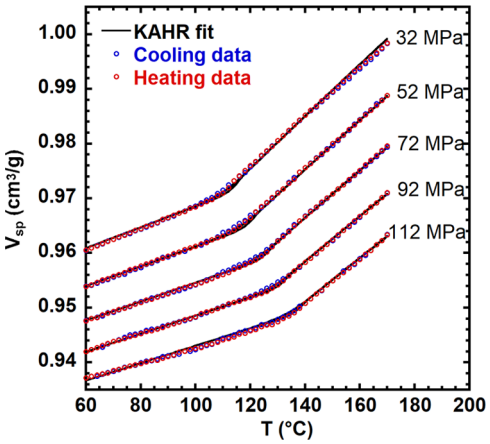

Figure 4. Predictions of the KAHR model for the isobaric cooling and heating scans at 32, 52, 72, 92, and 112 MPa. Also shown are the PVT data that are used for fitting the KAHR model.

Table 3. Values of the Adjustable KAHR Model Parameters

$\ln \tau_{ref}$	θ_T (K^{-1})	θ_P (MPa^{-1})	x	B
11.4	−0.670	0.199	0.525	0.613

(PVAc).[61] Our results for the two polystyrene PDGs are in good agreement with the literature results; those for two PEGs are the first two points in the literature for PS and agree with the literature for PVAc. Interestingly, the absolute value of the densification compressibility appears to be independent of the size or sign of pressure jump and to be approximately constant. Although this observation is not unexpected for a linear response, arguments from Weitz and Wunderlich[30] concerning the enhanced mobility in the PDG have suggested more than 30% volumetric relaxation during the pressure jump; such arguments seem to be fallacious given the observation of a constant densification compressibility.

In spite of the increased density of the PDG, in Figure 5, the heating scans for PDG-52 and PDG-72 show early devitrifications near 108 and 114 °C, respectively, with no noticeable overshoot, in comparison to the corresponding CGs that devitrify near 116 and 121 °C at 52 and 72 MPa, respectively. In addition, the slopes of glass lines show increased apparent thermal expansion coefficient in compar-

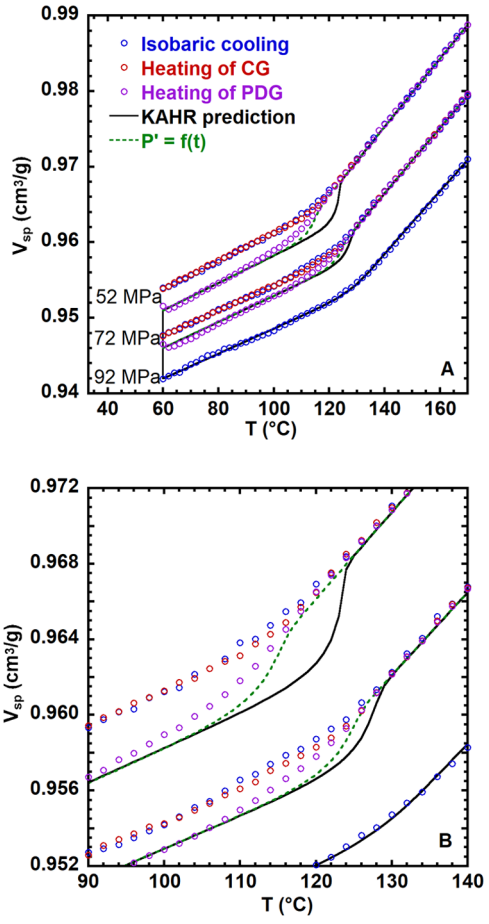

Figure 5. (A) PVT data for pressure down-jump experiments from P_1 = 92 MPa to P_2 = 52 and 72 MPa (purple markers), coupled with the data for isobaric cooling and heating scans at 52 and 72 MPA (red markers); blue markers are the corresponding cooling scans. The PVT data for pressure down-jumps to 72 MPa are averaged over three runs. Also shown are predictions of the conventional KAHR model on the pressure down-jump to 52 and 72 MPa (black solid lines), along with the predictions including the assumption of a time-dependent P' (green dotted lines). (B) Zoom-in view of the transition region shown in (A).

https://doi.org/10.1021/acs.macromol.1c00983
Macromolecules 2021, 54, 8352−8364

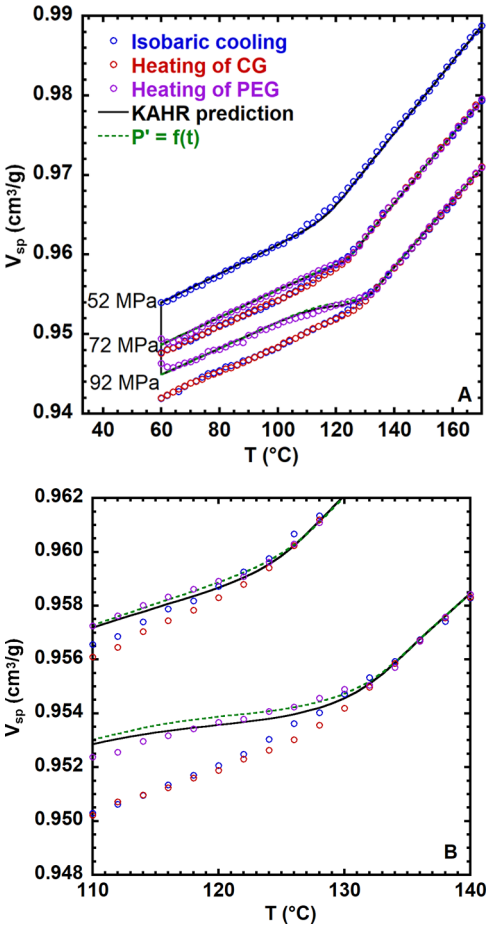

Figure 6. (A) PVT data for pressure up-jump experiments from P_1 = 52 MPa to P_2 = 72 and 92 MPa (purple markers), coupled with the data for isobaric cooling and heating scans at 72 and 92 MPA (red markers); blue markers are the corresponding cooling scans. The PVT data for pressure up-jumps to 72 MPa are averaged over three runs. Also shown are predictions of the conventional KAHR model on the pressure down-jump to 72 and 92 MPa (black solid lines), along with the predictions including the assumption of a time-dependent P' (green dotted lines). (B) Zoom-in view of the transition region shown in (A).

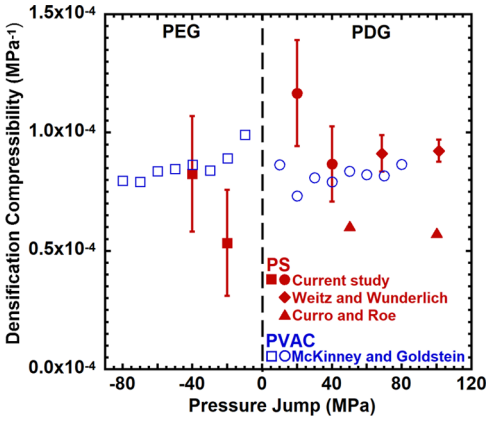

Figure 7. Densification compressibility for both the PDG and PEG using the volumetric data right after the pressure jump. Also shown are the densification compressibility calculated from the data of polystyrene (PS) in the literature: Weitz and Wunderlich,[30] and Curro and Roe,[43] as well as the data of poly(vinyl acetate) (PVAc) from McKinney and Goldstein.[61] Error bars are estimated from the uncertainty of the volumetric data.

ison to CGs. Both the early devitrification and higher α indicate increased mobility in the PDGs relative to CGs. Likewise, in Figure 6, the heating scans for PEG-72 and PEG-92 show early devitrification near 112 and 110 °C, respectively, in comparison to the corresponding CGs that devitrify near 121 and 129 °C at 52 and 72 MPa, respectively. In addition, the slopes of glass lines for the PEG show slightly decreased apparent α. These again indicate an increased mobility in PEGs compared to CGs. Notably, the data shown in Figures 5 and 6 for PDG-72 and PEG-72, respectively, are the average of three heating scans each in order to check the reproducibility of the nonisobaric thermal histories; the standard deviation of these three runs are also given in Table 1 and are the same order of magnitude as those for the isobaric experiments. At the beginning of each heating scan (near 60 °C) for PDGs and PEGs, a slight tip-up of the volume data is observed due to a backlash issue of the pressure-generation regulator; similar phenomena are observed for the isobaric cooling and heating scans below 50 °C. The KAHR model predictions, which are also shown in Figures 5 and 6, will be discussed shortly.

In order to determine the glassy response to pressure jump perturbations and to obtain $\Delta\beta$ for the KAHR model, isothermal pressure scans are conducted at 60 °C for two glasses from P_1 = 92 MPa toward P_2 = 52 MPa and from P_1 = 52 MPa toward P_2 = 72 MPa. The resulting volumetric data are plotted in Figure 8 versus pressure, where the PVT data for

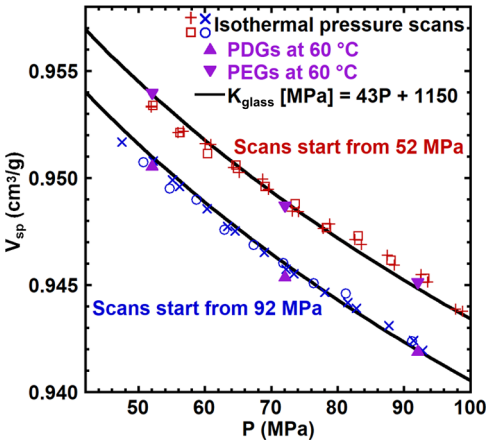

Figure 8. PVT data for isothermal pressure scans at 60 °C from 52 toward 92 MPa (red crosses and open squares) and from 92 toward 52 MPa (blue axes and open circles). The isothermal pressure scans are conducted before (open squares and circles) and after (crosses and axes) the PDG and PEG experiments. Also shown are the PVT data for PDGs (filled triangles) and PEGs (filled inverse triangles) at 60 °C, and the prediction using a linear function of glassy bulk modulus. The predictions using the linear bulk modulus function are referred to the pressure densification and expansion experiment data at 92 and 52 MPa for scans from 92 and 52 MPa, respectively.

PDGs and PEGs at 60 °C are also plotted and agree with the pressure scans. The pressure dependence of the glassy volume is well described by the bulk modulus as a linear function of pressure, K_{glass} [MPa] = 43P + 1150, as shown in Figure 8, giving a fitting error of ±0.00077 cm³/g.

The KAHR model can now be applied to predict the PVT data for the nonisobaric thermal histories, with the predictions shown as solid lines in Figures 5 and 6, for the pressure-

https://doi.org/10.1021/acs.macromol.1c00983
Macromolecules 2021, 54, 8352−8364

densified and pressure-expanded glasses, respectively. In both figures, the densities of the densified and expanded glasses at 60 °C are well predicted by the KAHR model with $\Delta\beta$ given by the liquid compressibility from the Tait equation and the linear glassy bulk modulus function from the experimental data, as mentioned above. On the other hand, the KAHR model predictions in Figure 5, for PDGs, show obvious overshoots and devitrification at temperatures above those where the corresponding CGs are devitrified, which disagrees with the experimentally observed unnoticeable overshoot and early devitrification. Thus, the KAHR model is unable to capture the increased mobility for the PDG using parameters that describe the PVT behavior for the CG. The KAHR model predictions in Figure 6, for PEGs, show early devitrifications in comparison to the corresponding CGs, which is in reasonable agreement with the data. However, the KAHR model cannot predict the slightly decreased apparent thermal expansion coefficient of glass lines (α_{glass}) during heating, as shown in Figure 6 for the PEG, and it similarly does not capture the increased α_{glass} for the PDG in Figure 5.

DISCUSSION

Although the KAHR model describes the pressure-dependent segmental mobility for isobaric cooling and heating scans, our results for the nonisobaric thermal histories indicate limitations of the KAHR model, particularly an inability to capture the increased mobility for the PDG. What are the missing physics? The conventional KAHR model assumes that the relaxation time depends on the departure from the instantaneous liquid state, $(V - V_e)/V_e$, as shown in eq 8 where the equilibrium volume, V_e, is a function of the instantaneous temperature and pressure. Thus, the PDG, having lower volume, V, than the corresponding CG, will have a smaller departure from equilibrium and reduced mobility, such that the model predicts an overshoot of the extrapolated liquid line on heating and devitrification later than the corresponding CG. However, studies by Weitz and Wunderlich[30] and Casalini and Roland[51] have suggested that the PDG has a high energy conformation corresponding to the liquid state where the glass was vitrified, thereby leading to an increased mobility in comparison to CG. From this perspective, we propose a novel modification of the KAHR model assuming that the PDG has a 'phantom' liquid state, V_e', that evolves with time from the liquid state where the glass was vitrified (at P_1) toward the liquid state where the glass is devitrified (at P_2). Therefore, V_e' is determined using the Tait equation in terms of the instantaneous temperature, T, and a time-dependent phantom pressure, P'

$$V_e' = V_e'(T, P') \tag{10}$$

For the conventional KAHR model, P' is equated to the instantaneous pressure after the pressure jump. When eq 10 is applied for the PDG, P' is still equated to P_1 immediately after the jump, leading to a larger δ in eqs 6 and 8, and thereby reducing the relaxation time.

In the present study, P' is assumed to relax from P_1 to P_2, starting after the pressure jump, t_{jump}, in a manner similar to the stretched exponential response function

$$P' = P_1 + (P_2 - P_1)[1 - \exp^{-((t-t_{jump})/\tau')^B}] \tag{11}$$

where the stretched exponent B is inherited from the KAHR model, *i.e.*, 0.613 in this work, and the overall constant relaxation time τ' is adjusted to best predict the PVT data during heating for the PDG. A similar method is used to also model the response of the PEG. The best predictions of this modification are shown in Figures 5 and 6, as dotted green lines, for PDGs and PEGs, respectively. For PDG-52 and PDG-72, this modification of a time-dependent P' significantly improves the ability to describe the early devitrification and lack of overshoot, using τ' of 16 000 and 14 000 s, respectively. For PEG-72 and PEG-92, this modification improves, albeit subtly since the conventional KAHR prediction was reasonable, the ability to describe the data during devitrification, using τ' of 9000 and 6000 s, respectively. The results of this modification corroborate the argument that the glass after a pressure jump remembers the liquid structure where it came from, i.e., the liquid from where it was vitrified before the pressure jump. The uncertainty of τ' is approximately ±1000 s for both the PDG and PEG, based on fitting with a 5% error imposed relative to the best fit. Although the τ' values for the PDG and PEG are of same order of magnitude in this study, differences among these values still quantitatively influence the result; we have assigned a universal τ' value of 10 000 s for all predictions, and the result becomes worse than the prediction using individual τ', with the prediction error increased by 7 and 22% for the glass after jumps of 20 and 40 MPa, respectively. In addition, we have noted that, when $P' = P_1$ up to devitrification, the simulated mobility is too fast for PDG-52 and PDG-72 resulting in an undershoot 43 and 28 °C below the nominal T_g, respectively, whereas the simulated mobility is too slow for PEG-72 and PEG-92 resulting in an overshoot 19 and 38 °C above the nominal T_g, respectively.

Although the modification of a time-dependent P' significantly facilitates describing the anomalous mobility during devitrification for the PDG, the increase in the coefficient of thermal expansion of glass lines (α_{glass}) during heating is still not captured with this modification, and neither is the slightly decreased α_{glass} for the PEG. The observed values of α_{glass} during heating for the CG, PDG, and PEG are quantified by linear fits to the heating data from 60 to 90 °C, and the results are summarized in Figure 9, along with those from the KAHR model predictions for the PDG and PEG. Apparently, the KAHR model underestimates α_{glass} of the PDG and overestimates that for the PEG. Moreover, in Figure 9, for PDG-52, the observed α_{glass} value is obviously higher than those for the CGs at 52 and 92 MPa; this stronger relaxation response in the glassy region cannot be obtained from the

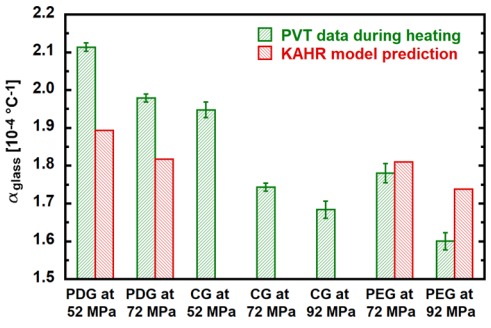

Figure 9. Coefficient of thermal expansion of glass lines (α_{glass}) during heating calculated from the PVT data for CG, PDG, and PEG, and from the KAHR model predictions for the PDG and PEG. The error of the apparent α_{glass} for the PVT data is propagated from the uncertainty of the PVT data given in Table 1.

https://doi.org/10.1021/acs.macromol.1c00983
Macromolecules 2021, 54, 8352−8364

phantom pressure-modified KAHR model; in fact, decreasing τ, relative to the phantom pressure-modified KAHR model prediction, results in greater underestimation of α_{glass} for the PDG. In addition, in Figure 9, for PEG-92, the observed α_{glass} value is lower than those for the CGs at 52 and 92 MPa; this weaker response obviously cannot be predicted unless the contraction associated with the pressurizing perturbation is stronger than the expansion associated with the heating perturbations.

Therefore, we turn to another limitation of the conventional KAHR model—the assumption that thermal and pressure perturbations have the same relaxation kinetics. Recently, Holt et al.[54] pointed out that this assumption may be the cause of the discrepancy between experimental observations and model predictions with respect to both the point of devitrification on heating and the "memory"-like behavior of a molecular PDG. Moreover, Santore et al.[89] have shown that the volumetric responses of thermal and mechanical stimuli for an epoxy glass relax with different time scales having a difference of at least two decades. So, we propose another modification of the KAHR model assuming that the pressure perturbations relax independently of the thermal perturbations, using two response functions, $M''(t, t')$ and $M(t, t')$ that are controlled by two independent relaxation times, τ'' and τ, respectively

$$V(t) = V_0 + \int V(t)\{\alpha_{glass} + \Delta\alpha[1 - M(t, t')]\}dT + \int V(t)\{\beta_{glass} + \Delta\beta[1 - M''(t, t')]\}dP \quad (12)$$

Here, the τ value is still calculated using eq 6, and the integral with respect to temperature is the volumetric contribution of the temperature perturbations and can be recorded for every numerical calculation step; the integral with respect to pressure is the contribution of the pressure perturbations. Thus, the value of τ'' is reverse-engineered, sequentially for each numerical calculation step after the pressure jump, by finding its value that best approximates the integral of pressure to be equal to the difference between $V(t)-V_0$ and the integral of temperature. This modification results in an excellent description of the data, including the observed thermal expansion coefficient of glass lines during heating and the early devitrification for PDG-52, giving a fitting error of ±0.00016. The logarithm of the representative reverse-engineered τ'' values for PDG-52 are plotted versus temperature in Figure 10, along with the τ values calculated using eq 6. For PDG-52, which undergoes a depressurization of 40 MPa, our τ'' value in the glassy state is approximately an order of magnitude larger than the volumetric relaxation time obtained for PS PDG by Weitz and Wunderlich[30] and Roe and Song,[42] both of which are $\sim 10^5$ s at 50 °C after pressure down-jumps of 276 and 300 MPa, respectively; notably, Roe and Song also showed that the effective relaxation rate for the PDG in the glassy state increased by approximately 1 decade as the pressure jump size increased by 150 MPa. Thus, our results are consistent with those of Weitz and Wunderlich[30] and Roe and Song.[42] The τ'' values in Figure 10 are obtained for the case when the KAHR model is not modified by the time-dependent P' for thermal perturbations, as well as for the case where the time-dependent P' modification is made; the corresponding τ'' profile is slightly modified, being 3% lower for the P' modification than that for the unmodified case in the glassy state, as shown in Figure 10. The 3% deviation is smaller than the error of the τ'' results in the glassy state, 7%, by at least 2-fold, and a student T-test indicates no statistically significant difference between the two τ'' values, with and without the P' modification; therefore, these two τ'' profiles are considered to be equivalent to one another in the glassy state, implying that the prediction of the observed α_{glass} for the PDG is obtained by the independent pressure and thermal relaxations.

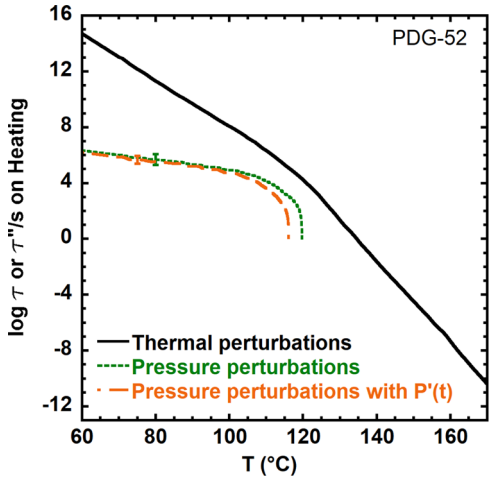

Figure 10. Relaxation time of the pressure perturbations (dotted line) that independently relaxes against that of the thermal perturbations (solid line) for the nonisobaric thermal histories of PDG-52. Also shown is the independent relaxation time of the pressure perturbations when a time-dependent P' is assumed for thermal perturbations (dashed line).

The modification of these independent relaxations between pressure and temperature perturbations also results in an excellent description of the data for PDG-72, PEG-72, and PEG-92, giving fitting errors of ±0.00012, ±0.00009, and ±0.00007 cm^3/g, respectively. For these three nonisobaric glasses, the τ'' results show behaviors qualitatively similar to the τ'' profile of the PDG-52 in Figure 10, *i.e.*, being 6−8 decades lower than τ at 60 °C and showing a weaker temperature dependence by 5-fold, and the τ'' values for the PEG-72 and PEG-92 merge with the τ values for $T > T_g - 18$ °C, which is not surprised as the two types of perturbations should relax with similar kinetics near and after reaching the equilibrium state. Quantitatively, in the glassy state, the τ'' values for PDG-72, PEG-72, and PEG-92 are different from those for the PDG-52 by −0.16 ± 0.05, 0.98 ± 0.11, and 0.35 ± 0.05 decades, respectively; the overall positive difference of the PEG to the PDG is possibly due to the fact that the magnitude of the relative decrease of α_{glass} for the PEG is smaller than that of the relative increase of α_{glass} for the PDG, as is shown in Figure 9, with relatively less contribution of the pressure perturbations needed for the relaxation of PEG.

In addition to the investigation of the thermal response on heating of the PDG and PEG, aging experiments have been conducted at 112 °C and 52 MPa after isobaric cooling from the liquid state for the CG, as well as after isobaric heating from 60 °C to 112 °C for PDG-52. The volumetric responses during aging are plotted in Figure 11 against the logarithm of aging time. In the case of aging of the CG, the normal contraction toward the equilibrium state is observed. For PDG, on the other hand, an initial expansion to the level of the CG is followed by a contraction, analogous to the Kovacs' memory experiment, as mentioned earlier. Holt et al.[54] have shown

https://doi.org/10.1021/acs.macromol.1c00983
Macromolecules 2021, 54, 8352−8364

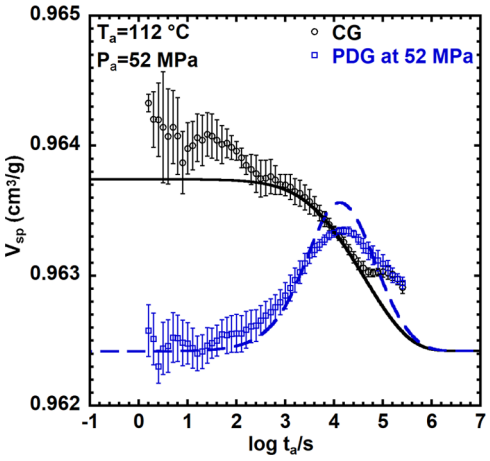

Figure 11. PVT data of the aging experiments at 112 °C and 52 MPa after isobarically cooling for a CG (black circles) or after isobarically heating from 60 °C to 112 °C for the PDG-52 (blue squares). Also shown are the predictions for the CG using the conventional KAHR model (black solid line) and for the PDG-52 using the KAHR model with the pressure perturbations independently relaxing assumed (blue dashed line).

similar observations for a molecular PDG, and their KAHR model using thermodynamic scaling shows a very subtle initial expansion and does not provide quantitative agreement with their data. We have applied the τ'' profile (without the time-dependent P') to predict the entire aging experiment in the present study for PDG-52, with the value of τ'' fixed when the material reaches 112 °C, and our method can quantitatively capture the signature of the "memory"-like volumetric response, which is shown in Figure 11 along with the prediction for the CG using the conventional KAHR model. The predictions of the equilibrium volume deviate from that of PVT data by roughly 0.0006 cm^3/g due to the long-term stability of the pressure signal. We also found that neither the conventional nor the P'-modified KAHR model could predict the initial expansion, consistent with the results of Holt et al.[54]

The Prigogine–Defay ratio[82,90−93] has been of interest for the thermodynamic description of glass-forming systems since the work of Davies and Jones[92] nearly 70 years ago. The ratio, defined as

$$\Pi \equiv \frac{\Delta C_p \Delta\beta}{TV\Delta\alpha} \tag{13}$$

is, by definition, equal to unity for a thermodynamic transition between two equilibrium states. However, the Prigogine–Defay ratio is typically found to be greater than unity for the glass transition (vitrification) and thought to indicate that the material is described by more than one ordering parameter, although Tropin et al.[91] showed that this interpretation is not the case for a lattice-hole model liquid. Interestingly, Colucci et al.[94] have pointed out that for isochoric vitrification, Π may be less than unity, emphasizing the problems that can arise when treating the kinetic vitrification process as a thermodynamic transition. Our PVT results can be used to estimate Π at atmospheric pressure, where T, V, $\Delta\alpha$, and β_{liquid} are calculated using Tait equation, β_{glass} is estimated by extrapolating the glassy bulk modulus at 60 °C to the atmospheric pressure, and ΔC_P is taken to be 0.29 J/(g K) as given by Badrinarayanan et al.[9] We find out that Π = 1.46 from our data, which is in reasonable agreement with values of 1.0 and 1.3 in the literature for polystyrene.[95−97]

CONCLUSIONS

In the present study, the segmental mobility of polystyrene pressure-densified glass and, for the first time, pressure-expanded glass is experimentally investigated during heating and isothermal aging, with the pressure and thermal cycles and volumetric measurement performed *in situ* using a custom-built pressurizable dilatometer. As expected, the PDG and PEG, respectively, show increased and decreased density with respect to the corresponding conventional glass. Moreover, both glasses show early devitrification on heating compared to the conventional glass, as well as an increase and slight decrease in the glassy thermal expansion coefficients for the PDG and PEG, respectively. These observations indicate that both the PDG and PEG have increased mobility relative to the conventional glass. In addition, the PDG shows a "memory"-like behavior during isothermal aging after heating to the temperature near the devitrification point.

The KAHR model of structural recovery is able to reasonably predict the early devitrification for the PEG, but the model fails with the PDG. The modeling results are improved by a modification that allows the relaxation time to depend on the departure from a phantom equilibrium state that initially depends on the liquid state where the glass was vitrified and that evolves toward the state where the glass is devitrified. On the other hand, neither the KAHR model nor this phantom state modification can describe the increased and slightly decreased α_{glass} during heating for the PDG and PEG, respectively. To capture this experimental observation, another modification was made to the KAHR model that allows the temperature and pressure perturbations to relax independently from one another. Moreover, this modification quantitatively predicts the "memory"-like aging behavior for the PDG.

ASSOCIATED CONTENT

Supporting Information

The Supporting Information is available free of charge at https://pubs.acs.org/doi/10.1021/acs.macromol.1c00983.

Bath temperature recorded as a function of time; experimental thermal expansion coefficient (α) in glass and liquid states as a function of temperature compared to the literature result; and experimental bulk modulus (K) in glass and liquid states as a function of temperature compared to the literature result (PDF)

AUTHOR INFORMATION

Corresponding Author

Sindee L. Simon − *Department of Chemical and Biomolecular Engineering, North Carolina State University, Raleigh, North Carolina 27695, United States;* orcid.org/0000-0001-7498-2826; Email: slsimon@ncsu.edu

Authors

Xiao Zhao − *Department of Chemical Engineering, Texas Tech University, Lubbock, Texas 79409, United States*

Luigi Grassia − *Department of Engineering, University of Campania Luigi Vanvitelli, Aversa 81031, Italy;* orcid.org/0000-0002-6796-9209

Complete contact information is available at: https://pubs.acs.org/10.1021/acs.macromol.1c00983

https://doi.org/10.1021/acs.macromol.1c00983
Macromolecules 2021, 54, 8352−8364

Notes

The authors declare no competing financial interest.

■ ACKNOWLEDGMENTS

The authors gratefully acknowledge funding from NSF-DMR 2004960.

■ REFERENCES

(1) McKenna, G. B.; Simon, S. L. 50th anniversary perspective: challenges in the dynamics and kinetics of glass-forming polymers. *Macromolecules* **2017**, *50*, 6333−6361.
(2) Ediger, M. D.; Angell, C. A.; Nagel, S. R. Supercooled liquids and glasses. *J. Phys. Chem. A* **1996**, *100*, 13200−13212.
(3) Angell, C. A. Thermodynamic aspects of the glass transition in liquids and plastic crystals. *Pure Appl. Chem.* **1991**, *63*, 1387−1392.
(4) Debenedetti, P. G.; Stillinger, F. H. Supercooled liquids and the glass transition. *Nature* **2001**, *410*, 259.
(5) Simon, S. L.; Sobieski, J. W.; Plazek, D. J. Volume and enthalpy recovery of polystyrene. *Polymer* **2001**, *42*, 2555−2567.
(6) Kovacs, A. J. Glass transition in amorphous polymers: a phenomenological study. *Adv. Polym. Sci.* **1963**, *3*, 394−508.
(7) Tool, A. Q. Relation between inelastic deformability and thermal expansion of glass in its annealing range. *J. Am. Ceram. Soc.* **1946**, *29*, 240−253.
(8) Moynihan, C. T.; Macedo, P. B.; Montrose, C. J.; Gupta, P. K.; DeBolt, M. A.; Dill, J. F.; Dom, B. E.; Drake, P. W.; Easteal, A. J.; Elterman, P. B.; Moeller, R. P.; Sasabe, H.; Wilder, J. A. Structural relaxation in vitreous materials. *Ann. N. Y. Acad. Sci.* **1976**, *279*, 15−35.
(9) Badrinarayanan, P.; Zheng, W.; Li, Q. X.; Simon, S. L. The glass transition temperature versus the fictive temperature. *J. Non-Cryst. Solids* **2007**, *353*, 2603−2612.
(10) Lopez, E.; Simon, S. L. Signatures of structural recovery in polystyrene by nanocalorimetry. *Macromolecules* **2016**, *49*, 2365−2374.
(11) Angell, C. A.; Ngai, K. L.; McKenna, G. B.; McMillan, P. F.; Martin, S. W. Relaxation in glassforming liquids and amorphous solids. *J. Appl. Phys.* **2000**, *88*, 3113−3157.
(12) Hutchinson, J. M. Physical aging of polymers. *Prog. Polym. Sci.* **1995**, *20*, 703−760.
(13) Hodge, I. M. Physical aging in polymer glasses. *Science* **1995**, *267*, 1945−1947.
(14) Tant, M. R.; Wilkes, G. L. Physical aging studies of semicrystalline poly (ethylene terephthalate). *J. Appl. Polym. Sci.* **1981**, *26*, 2813−2825.
(15) Aref-Azar, A.; Biddlestone, F.; Hay, J. N.; Haward, R. N. The effect of physical ageing on the properties of poly (ethylene terephthalate). *Polymer* **1983**, *24*, 1245−1251.
(16) Legrand, D. G. Crazing, yielding, and fracture of polymers. I. Ductile brittle transition in polycarbonate. *J. Appl. Polym. Sci.* **1969**, *13*, 2129−2147.
(17) Pan, P. J.; Zhu, B.; Inoue, Y. Enthalpy relaxation and embrittlement of poly (L-lactide) during physical aging. *Macromolecules* **2007**, *40*, 9664−9671.
(18) Kovacs, A. J.; Aklonis, J. J.; Hutchinson, J. M.; Ramos, A. R. Isobaric volume and enthalpy recovery of glasses. II. A transparent multiparameter theory. *J. Polym. Sci., Polym. Phys. Ed.* **1979**, *17*, 1097−1162.
(19) Narayanaswamy, O. S. A model of structural relaxation in glass. *J. Am. Ceram. Soc.* **1971**, *54*, 491−498.
(20) Svoboda, R.; Pustková, P.; Málek, J. Structural relaxation of polyvinyl acetate (PVAc). *Polymer* **2008**, *49*, 3176−3185.
(21) Koh, Y. P.; Simon, S. L. Enthalpy recovery of polystyrene: does a long-term aging plateau exist? *Macromolecules* **2013**, *46*, 5815−5821.
(22) Simon, S. L.; Park, J. Y.; McKenna, G. B. Enthalpy recovery of a glass-forming liquid constrained in a nanoporous matrix: negative pressure effects. *Eur. Phys. J. E* **2002**, *8*, 209−16.
(23) Grassia, L.; Simon, S. L. Modeling volume relaxation of amorphous polymers: Modification of the equation for the relaxation time in the KAHR model. *Polymer* **2012**, *53*, 3613−3620.
(24) Ramos, A. R.; Kovacs, A. J.; O'Reilly, J. M.; Tribone, J. J.; Greener, J. Effect of combined pressure and temperature changes on structural recovery of glass-forming materials. I. Extension of the KAHR model. *J. Polym. Sci., Part B: Polym. Phys.* **1988**, *26*, 501−513.
(25) Tribone, J. J.; O'Reilly, J. M.; Greener, J. Pressure-jump volume-relaxation studies of polystyrene in the glass transition region. *J. Polym. Sci., Part B: Polym. Phys.* **1989**, *27*, 837−857.
(26) Greener, J. Pressure-induced densification in injection molding. *Polym. Eng. Sci.* **1986**, *26*, 534−542.
(27) Johari, G. P.; Amann-Winkel, K.; Gainaru, C.; Handle, P. H.; Seidl, M.; Nelson, H.; Böhmer, R.; Loerting, T. Comment on "Water's second glass transitionProc. Natl. Acad. Sci. (U.S.) 110 (2013) 17720.", and the sub-Tg features of pressure-densified glasses. *Thermochim. Acta* **2015**, *617*, 208−218.
(28) Tammann, G.; Jenckel, E. Die Zunahme der dichte von gläsern nach erstarrung unter erhöhtem druck und die wiederkehr der natürlichen dichte durch temperatursteigerung. *Z. Anorg. Allg. Chem.* **1929**, *184*, 416−420.
(29) Andersson, O.; Johari, G. P. Sub-Tg features of glasses formed by cooling glycerol under pressure - Additional incompatibility of vibrational with configurational states in the depressurized, high density glass. *J. Chem. Phys.* **2016**, *145*, No. 204506.
(30) Weitz, A.; Wunderlich, B. Thermal analysis and dilatometry of glasses formed under elevated pressure. *J. Polym. Sci., Polym. Phys. Ed.* **1974**, *12*, 2473−2491.
(31) Allen, G.; Ayerst, R. C.; Cleveland, J. R.; Gee, G.; Price, C. Effect of conditions of glass formation on the density and energy of polystyrene. *J. Polym. Sci., Part C: Polym. Symp.* **1968**, *23*, 127−129.
(32) Oels, H.-J.; Rehage, G. Pressure-volume-temperature measurements on atactic polystyrene. A thermodynamic view. *Macromolecules* **1977**, *10*, 1036−1043.
(33) Wetton, R. E.; Moneypenny, H. G. Fundamental properties of densified polymeric glasses. *Br. Polym. J.* **1975**, *7*, 51−68.
(34) Kimmel, R. M.; Uhlmann, D. R. Effects of high pressure on amorphous polymers: densification of polymethyl methacrylate. *J. Appl. Phys.* **1970**, *41*, 2917−2927.
(35) Schmidt, M.; Maurer, F. H. Isotropic pressure-densified atactic poly (methyl methacrylate) glasses: Free-volume properties from equation-of-state data and positron annihilation lifetime spectroscopy. *Macromolecules* **2000**, *33*, 3879−3891.
(36) Casalini, R.; Roland, C. M. Communication: Effect of density on the physical aging of pressure-densified polymethylmethacrylate. *J. Chem. Phys.* **2017**, *147*, No. 091104.
(37) Bree, H. W.; Heijboer, J.; Struik, L. C. E.; Tak, A. G. M. The effect of densification on the mechanical properties of amorphous glassy polymers. *J. Polym. Sci., Polym. Phys. Ed.* **1974**, *12*, 1857−1864.
(38) Holt, A. P.; Fragiadakis, D.; Wollmershauser, J. A.; Feigelson, B. N.; Tyagi, M.; Roland, C. M. Stability limits of pressure densified polycarbonate glass. *Macromolecules* **2019**, *52*, 4139−4144.
(39) Dale, W. C.; Rogers, C. E. Mechanical and relaxation properties of polystyrene molded at high pressures. *J. Appl. Polym. Sci.* **1972**, *16*, 21−36.
(40) Brown, I. G.; Wetton, R. E.; Richardson, M. J.; Savill, N. G. Glass transition and thermodynamic state of densified polymeric glasses. *Polymer* **1978**, *19*, 659−663.
(41) Yourtee, J. B.; Cooper, S. L. Properties of densified amorphous polystyrene. *J. Appl. Polym. Sci.* **1974**, *18*, 897−912.
(42) Roe, R. J.; Song, H. H. Isothermal relaxation of volume and density fluctuation of polystyrene glass prepared under pressure. *Macromolecules* **1985**, *18*, 1603−1609.
(43) Curro, J. J.; Roe, R. J. Small-angle x-ray scattering study of density fluctuation in pressure-densified polystyrene glasses. *J. Polym. Sci., Polym. Phys. Ed.* **1983**, *21*, 1785−1796.
(44) Song, H. H.; Roe, R. J. Structural change accompanying volume change in amorphous polystyrene as studied by small and

https://doi.org/10.1021/acs.macromol.1c00983
Macromolecules 2021, 54, 8352−8364

intermediate angle X-ray scattering. *Macromolecules* **1987**, *20*, 2723−2732.
(45) Floudas, G.; Pakula, T.; Stamm, M.; Fischer, E. W. Density fluctuations in bisphenol A polycarbonate and tetramethyl bisphenol A polycarbonate as studied by x-ray diffraction. *Macromolecules* **1993**, *26*, 1671−1675.
(46) Prest, W. M., Jr.; O'Reilly, J. M.; Roberts, F. J., Jr.; Mosher, R. A. Non-equilibrium processes in poly (vinyl chloride) glasses vitrified at elevated pressures. *Polym. Eng. Sci.* **1981**, *21*, 1181−1187.
(47) Vijayan, K.; Tang, C.-L.; Pae, K. D. Effect of physical ageing on mechanical behaviour of an elastomeric glass under combined pressure and temperature. *Polymer* **1988**, *29*, 396−404.
(48) Pae, K. D.; Vijayan, K. Memory behaviour of an elastomeric glass by pressure-and temperature-perturbation methods. *Polymer* **1988**, *29*, 405−409.
(49) Destruel, P.; Ai, B.; Hoang-The-Giam. Dielectric results of polymeric glasses formed under hydrostatic pressure: Is the densified sample closer to thermodynamic equilibrium? *J. Appl. Phys.* **1984**, *55*, 2726−2732.
(50) Casalini, R.; Roland, C. M. Pressure densification of a simple liquid. *J. Non-Cryst. Solids* **2017**, *475*, 25−27.
(51) Casalini, R.; Roland, C. M. Anomalous properties of the local dynamics in polymer glasses. *J. Chem. Phys.* **2009**, *131*, No. 114501.
(52) Johari, G. P.; Andersson, O. Structural relaxation and thermal conductivity of high-pressure formed, high-density di-n-butyl phthalate glass and pressure induced departures from equilibrium state. *J. Chem. Phys.* **2017**, *146*, No. 234505.
(53) Kimmel, R. M.; Uhlmann, D. R. Effects of pressure on amorphous polymers. III. Thermodynamic properties of densified polymethyl methacrylate. *J. Appl. Phys.* **1971**, *42*, 4917−4925.
(54) Holt, A. P.; Fragiadakis, D.; Roland, C. M. Pressure densified 1, 3, 5-tri (1-naphthyl) benzene glass. I. Volume recovery and physical aging. *J. Chem. Phys.* **2019**, *151*, No. 184502.
(55) Schmidt, M.; Olsson, M.; Maurer, F. H. Macroscopic pressure−volume−temperature properties versus free-volume characteristics of isotropic pressure-densified amorphous polymer glasses. *J. Chem. Phys.* **2000**, *112*, 11095−11106.
(56) Hofer, K.; Perez, J.; Johari, G. P. Detecting enthalpy 'cross-over'in vitrified solids by differential scanning calorimetry. *Philos. Mag. Lett.* **1991**, *64*, 37−43.
(57) Bernazzani, P.; Simon, S. L. Volume recovery of polystyrene: evolution of the characteristic relaxation time. *J. Non-Cryst. Solids* **2002**, *307*−*310*, 470−480.
(58) Hirai, N.; Eyring, H. Bulk viscosity of polymeric systems. *J. Polym. Sci.* **1959**, *37*, 51−70.
(59) Casalini, R.; Roland, C. M. Thermodynamical scaling of the glass transition dynamics. *Phys. Rev. E* **2004**, *69*, No. 062501.
(60) Bianchi, U.; Turturro, A.; Basile, G. Pressure effects on glass transition in polymers. II. A study of the factors affecting dT_g/dP values. *J. Phys. Chem. A* **1967**, *71*, 3555−3558.
(61) McKinney, J. E.; Goldstein, M. PVT relationships for liquid and glassy poly (vinyl acetate). *J. Res. Natl. Bur. Stand., Sect. A* **1974**, *78A*, 331.
(62) Quach, A.; Simha, R. Pressure-volume-temperature properties and transitions of amorphous polymers; polystyrene and poly (orthomethylstyrene). *J. Appl. Phys.* **1971**, *42*, 4592−4606.
(63) Zoller, P. A study of the pressure-volume-temperature relationships of four related amorphous polymers: Polycarbonate, polyarylate, phenoxy, and polysulfone. *J. Polym. Sci., Polym. Phys. Ed.* **1982**, *20*, 1453−1464.
(64) Walsh, D.; Zoller, P. *Standard Pressure Volume Temperature Data for Polymers*; CRC Press, 1995.
(65) Ougizawa, T.; Dee, G. T.; Walsh, D. J. Pressure-volume-temperature properties and equations of state in polymer blends: characteristic parameters in polystyrene/poly (vinyl methyl ether) mixtures. *Macromolecules* **1991**, *24*, 3834−3837.
(66) Sato, Y.; Yamasaki, Y.; Takishima, S.; Masuoka, H. Precise measurement of the PVT of polypropylene and polycarbonate up to 330 C and 200 MPa. *J. Appl. Polym. Sci.* **1997**, *66*, 141−150.
(67) Lei, M.; Reid, C. G.; Zoller, P. Stresses and volume changes in a polymer loaded axially in a rigid die. *Polymer* **1988**, *29*, 1784−1788.
(68) Meng, Y.; Simon, S. L. Pressure relaxation of polystyrene and its comparison to the shear response. *J. Polym. Sci., Part B: Polym. Phys.* **2007**, *45*, 3375−3385.
(69) Meng, Y.; Bernazzani, P.; O'Connell, P. A.; McKenna, G. B.; Simon, S. L. A new pressurizable dilatometer for measuring the time-dependent bulk modulus and pressure-volume-temperature properties of polymeric materials. *Rev. Sci. Instrum.* **2009**, *80*, No. 053903.
(70) Guo, J. X.; Grassia, L.; Simon, S. L. Bulk and shear rheology of a symmetric three-arm star polystyrene. *J. Polym. Sci., Part B: Polym. Phys.* **2012**, *50*, 1233−1244.
(71) Guo, J. X.; Simon, S. L. Effect of crosslink density on the pressure relaxation response of polycyanurate networks. *J. Polym. Sci., Part B: Polym. Phys.* **2009**, *47*, 2477−2486.
(72) Guo, J. X.; Simon, S. L. Pressure-volume-temperature behavior of two polycyanurate networks. *J. Polym. Sci., Part B: Polym. Phys.* **2010**, *48*, 2509−2517.
(73) Tao, R.; Simon, S. L. Bulk and shear rheology of silica/polystyrene nanocomposite: Reinforcement and dynamics. *J. Polym. Sci., Part B: Polym. Phys.* **2015**, *53*, 621−632.
(74) Tao, R.; Simon, S. L. Pressure-volume-temperature and glass transition behavior of silica/polystyrene nanocomposite. *J. Polym. Sci., Part B: Polym. Phys.* **2015**, *53*, 1131−1138.
(75) Struik, L. C. E. *Physical Aging in Polymers and Other Amorphous Materials*; Elsevier: Amsterdam, 1976.
(76) Tait, P. G. *Physics and Chemistry of the Voyage of H.M.S. Challenger*; HMSO: London, 1888; Vol. *2*.
(77) Dymond, J. H.; Malhotra, R. The Tait equation: 100 years on. *Int. J. Thermophys.* **1988**, *9*, 941−951.
(78) Orwoll, R. A. Densities, Coefficients of Thermal Expansion, and Compressibilities of Amorphous Polymers. In *Physical Properties of Polymers Handbook*; Springer, 2007; pp 93−101.
(79) Zhao, X.; Simon, S. L. A model-free analysis of configurational properties to reduce the temperature- and pressure-dependent segmental relaxation times of polymers. *J. Chem. Phys.* **2020**, *152*, No. 044901.
(80) Kohlrausch, R. Theorie des elektrischen Rückstandes in der Leidener Flasche. *Ann. Phys. Chem.* **1854**, *167*, 179−214.
(81) Williams, G.; Watts, D. C. Non-symmetrical dielectric relaxation behaviour arising from a simple empirical decay function. *Trans. Faraday Soc.* **1970**, *66*, 80−85.
(82) Hodge, I. M. Enthalpy relaxation and recovery in amorphous materials. *J. Non-Cryst. Solids* **1994**, *169*, 211−266.
(83) McKinney, J. E.; Simha, R. Thermodynamics of the densification process for polymer glasses. *J. Res. Natl. Bur. Stand., Sect. A* **1977**, *81A*, 283−297.
(84) Roland, C. M.; Casalini, R. Temperature dependence of local segmental motion in polystyrene and its variation with molecular weight. *J. Chem. Phys.* **2003**, *119*, 1838−1842.
(85) Utracki, L. A. Pressure−volume−temperature of molten and glassy polymers. *J. Polym. Sci., Part B: Polym. Phys.* **2007**, *45*, 270−285.
(86) Zoller, P.; Hoehn, H. H. Pressure-volume-temperature properties of blends of poly (2, 6-dimethyl-1, 4-phenylene ether) with polystyrene. *J. Polym. Sci., Polym. Phys. Ed.* **1982**, *20*, 1385−1397.
(87) Hutchinson, J. M.; Ruddy, M. Thermal cycling of glasses. II. Experimental evaluation of the structure (or nonlinearity) parameter x. *J. Polym. Sci., Part B: Polym. Phys.* **1988**, *26*, 2341−2366.
(88) Li, Q. X.; Simon, S. L. Enthalpy recovery of polymeric glasses: Is the theoretical limiting liquid line reached? *Polymer* **2006**, *47*, 4781−4788.
(89) Santore, M. M.; Duran, R. S.; McKenna, G. B. Volume recovery in epoxy glasses subjected to torsional deformations: the question of rejuvenation. *Polymer* **1991**, *32*, 2377−2381.
(90) Schmelzer, J. W. P.; Gutzow, I. The prigogine-defay ratio revisited. *J. Chem. Phys.* **2006**, *125*, No. 184511.
(91) Tropin, T. V.; Schmelzer, J. W.; Schick, C. On the dependence of the properties of glasses on cooling and heating rates II: Prigogine−

https://doi.org/10.1021/acs.macromol.1c00983
Macromolecules 2021, 54, 8352−8364

Defay ratio, fictive temperature and fictive pressure. *J. Non-Cryst. Solids* **2011**, *357*, 1303−1309.
(92) Davies, R. O.; Jones, G. O. The irreversible approach to equilibrium in glasses. *Proc. R. Soc. London, Ser. A* **1953**, *217*, 26−42.
(93) Gupta, P. K.; Moynihan, C. T. Prigogine−Defay ratio for systems with more than one order parameter. *J. Chem. Phys.* **1976**, *65*, 4136−4140.
(94) Colucci, D. M.; McKenna, G. B.; Filliben, J. J.; Lee, A.; Curliss, D. B.; Bowman, K. B.; Russell, J. D. Isochoric and isobaric glass formation: Similarities and differences. *J. Polym. Sci., Part B: Polym. Phys.* **1997**, *35*, 1561−1573.
(95) Nieuwenhuizen, T. M. Formulation of thermodynamics for the glassy state: configurational energy as a modest source of energy. *J. Chem. Phys.* **2001**, *115*, 8083−8088.
(96) Gundermann, D.; Pedersen, U. R.; Hecksher, T.; Bailey, N. P.; Jakobsen, B.; Christensen, T.; Olsen, N. B.; Schrøder, T. B.; Fragiadakis, D.; Casalini, R.; Roland, C. M.; Dyre, J. C.; Niss, K. Predicting the density-scaling exponent of a glass-forming liquid from Prigogine−Defay ratio measurements. *Nat. Phys.* **2011**, *7*, 816−821.
(97) Takahara, S.; Ishikawa, M.; Yamamuro, O.; Matsuo, T. Structural relaxations of glassy polystyrene and o-terphenyl studied by simultaneous measurement of enthalpy and volume under high pressure. *J. Phys. Chem. B* **1999**, *103*, 792−796.

https://doi.org/10.1021/acs.macromol.1c00983
Macromolecules 2021, 54, 8352−8364